EXTENDED PDF FORMAT
SPONSORED BY
More Differentiation. With Less Variation.
Reduce Variation in Your Stem Cell Experiments.
R&D SYSTEMS
www.rndsystems.com

Coherence and Indistinguishability of Single Electrons Emitted by Independent Sources

E. Bocquillon *et al.*

Science **339**, 1054 (2013);
DOI: 10.1126/science.1232572

This copy is for your personal, non-commercial use only.

If you wish to distribute this article to others, you can order high-quality copies for your colleagues, clients, or customers by clicking here.

Permission to republish or repurpose articles or portions of articles can be obtained by following the guidelines here.

The following resources related to this article are available online at www.sciencemag.org (this information is current as of March 21, 2013):

Updated information and services, including high-resolution figures, can be found in the online version of this article at:
http://www.sciencemag.org/content/339/6123/1054.full.html

A list of selected additional articles on the Science Web sites **related to this article** can be found at:
http://www.sciencemag.org/content/339/6123/1054.full.html#related

This article **cites 29 articles**, 3 of which can be accessed free:
http://www.sciencemag.org/content/339/6123/1054.full.html#ref-list-1

This article appears in the following **subject collections:**
Physics
http://www.sciencemag.org/cgi/collection/physics

Downloaded from www.sciencemag.org on March 21, 2013

Science (print ISSN 0036-8075; online ISSN 1095-9203) is published weekly, except the last week in December, by the American Association for the Advancement of Science, 1200 New York Avenue NW, Washington, DC 20005. Copyright 2013 by the American Association for the Advancement of Science; all rights reserved. The title *Science* is a registered trademark of AAAS.

10. R. L. Compton, P. A. Crowell, *Phys. Rev. Lett.* **97**, 137202 (2006).
11. R. L. Compton, T. Y. Chen, P. A. Crowell, *Phys. Rev. B* **81**, 144412 (2010).
12. J. S. Kim *et al.*, *Phys. Rev. B* **82**, 104427 (2010).
13. T. Y. Chen, A. T. Galkiewicz, P. A. Crowell, *Phys. Rev. B* **85**, 180406 (2012).
14. S. S. P. Parkin, M. Hayashi, L. Thomas, *Science* **320**, 190 (2008).
15. D. A. Allwood *et al.*, *Science* **309**, 1688 (2005).
16. J. H. Franken, H. J. M. Swagten, B. Koopmans, *Nat. Nanotechnol.* **7**, 499 (2012).
17. H. Min, R. D. McMichael, M. J. Donahue, J. Miltat, M. D. Stiles, *Phys. Rev. Lett.* **104**, 217201 (2010).
18. M. Eltschka *et al.*, *Phys. Rev. Lett.* **105**, 056601 (2010).
19. C. Chappert *et al.*, *Science* **280**, 1919 (1998).
20. J. Moreland, *J. Phys. D Appl. Phys.* **36**, R39 (2003).
21. J. P. Davis *et al.*, *J. Appl. Phys.* **109**, 07D309 (2011).
22. Supplementary materials are available on *Science* Online.
23. J. A. J. Burgess, J. E. Losby, M. R. Freeman, http://arxiv.org/abs/1208.3797 (2012).
24. K. Y. Guslienko, V. Novosad, Y. Otani, H. Shima, K. Fukamichi, *Phys. Rev. B* **65**, 024414 (2001).
25. J. A. J. Burgess *et al.*, *Phys. Rev. B* **82**, 144403 (2010).
26. K. Y. Guslienko *et al.*, *J. Appl. Phys.* **91**, 8037 (2002).
27. K. L. Metlov, K. Y. Guslienko, *J. Magn. Magn. Mater.* **242**, 1015 (2002).
28. M. Rahm, J. Stahl, W. Wegscheider, D. Weiss, *Appl. Phys. Lett.* **85**, 1553 (2004).
29. M. Rahm, R. Höllinger, V. Umansky, D. Weiss, *J. Appl. Phys.* **95**, 6708 (2004).
30. R. Zarzuela, S. Vélez, J. M. Hernandez, J. Tejada, V. Novosad, *Phys. Rev. B* **85**, 180401 (2012).
31. G. Mihajlovic *et al.*, *Appl. Phys. Lett.* **96**, 112501 (2010).

Acknowledgments: This work was supported by the Natural Sciences and Engineering Research Council, Canada, the Canadian Institute for Advanced Research, the Informatics Circle of Research Excellence, Canada Research Chairs, the Integrated Nanosystems Research Facility, the Canadian Foundation for Innovation, nanoAlberta, and the National Institute for Nanotechnology. The samples were fabricated using the electron microscopy facilities of the National Institute for Nanotechnology and Infrastructure of the Centre for Nanoscale Physics and Nanomaterials Research at the University of Alberta. J.B. thanks the Alberta Ingenuity Foundation/Alberta Innovates for support. We are grateful to W. Hiebert, J. Losby, Z. Diao, M. Malac, and V. Sauer for many discussions; to P. Li for TEM work; and to D. Fortin for technical assistance.

Supplementary Materials

www.sciencemag.org/cgi/content/full/science.1231390/DC1
Materials and Methods
Supplementary Text
Figs. S1 to S7
Movies S1 to S3
References (*32*–*40*)

11 October 2012; accepted 17 December 2012
Published online 17 January 2013;
10.1126/science.1231390

Coherence and Indistinguishability of Single Electrons Emitted by Independent Sources

E. Bocquillon,[1] V. Freulon,[1] J.-M Berroir,[1] P. Degiovanni,[2] B. Plaçais,[1] A. Cavanna,[3] Y. Jin,[3] G. Fève[1]*

The on-demand emission of coherent and indistinguishable electrons by independent synchronized sources is a challenging task of quantum electronics, in particular regarding its application for quantum information processing. Using two independent on-demand electron sources, we triggered the emission of two single-electron wave packets at different inputs of an electronic beam splitter. Whereas classical particles would be randomly partitioned by the splitter, we observed two-particle interference resulting from quantum exchange. Both electrons, emitted in indistinguishable wave packets with synchronized arrival time on the splitter, exited in different outputs as recorded by the low-frequency current noise. The demonstration of two-electron interference provides the possibility of manipulating coherent and indistinguishable single-electron wave packets in quantum conductors.

As with photons, the wave-particle duality plays a crucial role in the propagation of electrons in quantum conductors. The wave nature of electrons can be revealed in interference experiments (*1*–*3*) probing the single-particle coherence of electron sources through the measurement of the average electrical current. The corpuscular nature of charge carriers is apparent when measuring fluctuations of the electrical current (*4*). Yet, some experiments cannot be understood within the wave or the corpuscular description. This is the case when two-particle interference effects related to the exchange between two indistinguishable particles take place. Such experiments have proven particularly interesting—both from a fundamental standpoint, as they require a full quantum treatment, and because the on-demand generation of indistinguishable partners is at the heart of quantum information protocols (*5*). Information coding in few-electron states that propagate ballistically in quantum conductors (*6*) thus requires the production of coherent and indistinguishable single-particle wave packets emitted by several synchronized but otherwise independent emitters. The collision of two particles emitted at two different inputs of a beam splitter can be used to measure their degree of indistinguishability. In the case of bosons, indistinguishable partners always exit in the same output (Fig. 1). Fermionic statistics leads to the opposite behavior: Particles exit in different outputs. The bunching of indistinguishable photons has been observed by recording the coincidence counts between two detectors placed at the outputs of the beam splitter as a function of the time delay τ between the arrival times of the photons on the splitter. Bunching shows up in a dip in the coincidence counts, the Hong-Ou-Mandel (HOM) dip (*7*), when τ is varied. The reduction of the coincidence counts directly measures the overlap between the single-particle states at the input. It is maximum when the arrivals are synchronized and can be suppressed when the delay becomes larger than the wave-packet widths.

The production of indistinguishable partners is challenging, and their generation by independent sources has only recently been achieved in optics (*8*). In one-dimensional quantum conductors, a continuous stream of indistinguishable electrons can be produced by applying a dc voltage bias to two different electronic reservoirs. Because of fermionic statistics, each source fills the electronic states up to the chemical potential $-eV$, and identical electron beams are generated. With the use of such sources, the π exchange phase of indistinguishable fermions has been measured in the above-described collider geometry (*9*) and in a two-particle interferometer based on a Mach-Zehnder geometry (*10*, *11*). However, as these sources generate a continuous beam of electrons, they do not reach the single-particle resolution of their optical analog, and two-particle interference cannot be interpreted as resulting from the overlap between two single-particle wave packets. The manipulation of single-particle states thus requires replacement of dc emitters by triggered ac emitters that generate a single-electron wave packet at a well-defined time.

When dealing with electrons, one can benefit from the charge quantization of a small quantum dot enforced both by Coulomb interaction and fermionic statistics to trigger the emission of particles one by one (*12*–*16*). Moreover, the edge channels of the quantum Hall effect provide an ideal test bench to implement optic-like experiments with electron beams in condensed matter, as electron propagation is ballistic, one-dimensional, and chiral. We will consider here a mesoscopic capacitor (*12*), which comprises a small quantum dot capacitively coupled to a metallic top gate and tunnel coupled to a single edge channel by a quantum point contact of variable transmission D. By applying a square-wave periodic radiofrequency excitation on the top gate, whose

[1]Laboratoire Pierre Aigrain, Ecole Normale Supérieure, CNRS (UMR8551), Université Pierre et Marie Curie, Université Paris Diderot, 24 rue Lhomond, 75231 Paris Cedex 05, France. [2]Université de Lyon, Fédération de Physique André Marie Ampère, CNRS–Laboratoire de Physique de l'Ecole Normale Supérieure de Lyon 46 Allée d'Italie, 69364 Lyon Cedex 07, France. [3]CNRS–Laboratoire de Photonique et de Nanostructures Route de Nozay, 91460 Marcoussis, France.

*To whom correspondence should be addressed. E-mail: feve@lpa.ens.fr

Downloaded from www.sciencemag.org on March 21, 2013

peak-to-peak amplitude matches the dot addition energy, $2eV_{exc} \approx \Delta$, a quantized current resulting from the emission of a single electron followed by a single hole is generated (*12*). Beyond average current measurements, this emitter has been characterized through the study of current correlations on short times (*17*–*20*) as well as partition noise measurements (*21*) in the electronic analog of the Hanbury-Brown and Twiss geometry (*22*, *23*). These measurements have demonstrated that, for escape times smaller than half the period of the excitation drive, exactly a single-electron and a single-hole excitation were successively emitted at each period. Moreover, the tunnel emission of single particles from a discrete dot level should lead to electron and hole wave functions described by exponentially decaying wave packets (*24*, *25*): $\phi(t) = \frac{1}{\sqrt{\tau_e}}\Theta(t - t_0)e^{i\frac{\Delta(t-t_0)}{2\hbar}}e^{-\frac{t-t_0}{2\tau_e}}$, where $\Theta(t)$ is the step function, $\Delta/2$ is the energy of emitted electrons and holes, and t_0 is the emission trigger that can be tuned with an accuracy of a few picoseconds. Measurements of the average current $\langle I(t)\rangle$ (*12*) and short-time correlations $\langle I(t)I(t+\tau)\rangle$ (*17*) have confirmed that the probability of single-particle detection (that is, the envelope of the wave packet) was following this exponential decay. However, these measurements are only sensitive to the squared modulus of the wave function, $|\phi(t)|^2$, and as such, do not probe the coherence of the electronic wave packet related to the phase relationship between $\phi(t)$ and $\phi^*(t')$ (for $t \neq t'$) and encoded in the off-diagonal components (coherences) of the density matrix $\rho(t,t') = \phi(t)\phi^*(t')$.

When two such emitters are used at the two inputs of an electronic beam splitter, the coherence and indistinguishability of two single electronic wave packets can be probed by two-electron interference (*25*–*27*). Considering the electron emission sequence, each emitter generates an electronic wave packet $|\phi_i\rangle$ ($i = 1, 2$) above the Fermi energy at each input of the splitter set at transmission $\mathcal{T} = 1/2$. The probability $P(1,1)$ that the two particles exit in different outputs is related to the overlap between wave packets: $P(1,1) = \frac{1}{2}\left[1 + |\langle\phi_1|\phi_2\rangle|^2\right]$. An opposite sign occurs in the expression of the probability that both particles exit in the same output, $P(0,2) + P(2,0) = \frac{1}{2}\left[1 - |\langle\phi_1|\phi_2\rangle|^2\right]$. These signs are related to the exchange phase of π for fermions; they would be opposite for bosons. For fermions, the coincidence counts for indistinguishable particles would thus be doubled compared to the classical case (Fig. 1). However, single-shot detection of ballistic electrons in condensed matter is not available. Antibunching is thus probed not by coincidence counts but rather by low-frequency fluctuations of the electrical current in the outputs related to the fluctuations of the number of transmitted particles: $\langle\delta N_3^2\rangle = \langle\delta N_4^2\rangle = \frac{1}{2}\left[1 - |\langle\phi_1|\phi_2\rangle|^2\right]$. Repeating this two-electron collision at frequency f and considering the successive emission of one electron and one hole per period, the low-frequency current noise at the output is then given by (*25*)

$$S_{33} = S_{44} = e^2 f \times \left[1 - |\langle\phi_1|\phi_2\rangle|^2\right] \quad (1)$$

$$= e^2 f \times \left[1 - \left|\int dt\,\phi_1(t)\phi_2^*(t)\right|^2\right] \quad (2)$$

The single-electron wave packets ϕ_i in Eq. 2 differ from the states generated by applying a time-dependent voltage $V_i(t)$ on each electronic reservoir connected to inputs $i = 1,2$ and cannot be generated by such classical drive [in which case, the two inputs in Eq. 2 can be reduced to a single one by the proper gauge transformation that shifts the potentials by $V(t) = V_2(t)$]. For perfectly indistinguishable states, $\phi_2(t) = \phi_1(t)$, a complete suppression of the output noise is obtained. By delaying by time τ the emission of one particle with respect to the other, $\phi_2(t) = \phi_1(t + \tau)$, the full random partitioning of classical particles $S_{33} = S_{44} = e^2 f$ can be recovered (Fig. 1). It is thus convenient to consider the noise normalized by the classical random partitioning $q = S_{44}/e^2 f$, which equals for exponentially decaying wave packets

$$q = 1 - e^{-|\tau|/\tau_e} \quad (3)$$

Equation 3 is valid at zero temperature, or when the Fourier components of the wave functions $\tilde{\phi}_i(\omega)$ have no overlap with the thermal excitations: $\tilde{\phi}_i(\omega) = 0$ for $\hbar\omega \approx k_B T$. Otherwise, the random partitioning is also affected by antibunching with the thermal excitations, so that $S_{44} \leq e^2 f$ (*21*). However, if one measures the normalized value of the excess noise Δq between the situations where both sources are switched on and switched off, simulations describing the source in the Floquet scattering formalism (*20*, *28*) show that Δq is accurately described by Eq. 3 for moderate temperatures $k_B T << \Delta$.

The circuit (Fig. 2), is realized in a two-dimensional electron gas at a AlGaAs/GaAs heterojunction, of nominal density $n = 1.9 \times 10^{15}$ m^{-2} and mobility $\mu = 2.4 \times 10^6$ cm^2 V^{-1} s^{-1}. A strong magnetic field $B = 2.68$ T is applied so as to work in the quantum Hall regime at filling factor $\nu = 3$ ($\nu = 3$ is chosen because, in this sample, the splitter transparency $\mathcal{T}$ becomes energy dependent at higher values of the magnetic field). Two mesoscopic capacitors with identical addition energies $\Delta = 1.4$ K (much larger than the electronic temperature $T = 100$ mK) are used as electron and hole emitters and placed at a 3-μm distance from a quantum point contact used as an electronic beam splitter at transmission $\mathcal{T} = \frac{1}{2}$. Single-charge emission in the outer edge channel is triggered with a square excitation at frequency $f = 2.1$ GHz with average emission times set to $\tau_{e,1} = \tau_{e,2} = 58 \pm 7$ ps, corresponding to a transmission $D_1 = D_2 = 0.45 \pm 0.05$. The low-frequency partition noise is measured at output 4. Figure 3 presents the measurements of Δq as a function of the time delay τ between the two sources. We observe a dip in the noise measurements for zero time delay and a plateau for longer

Downloaded from www.sciencemag.org on March 21, 2013

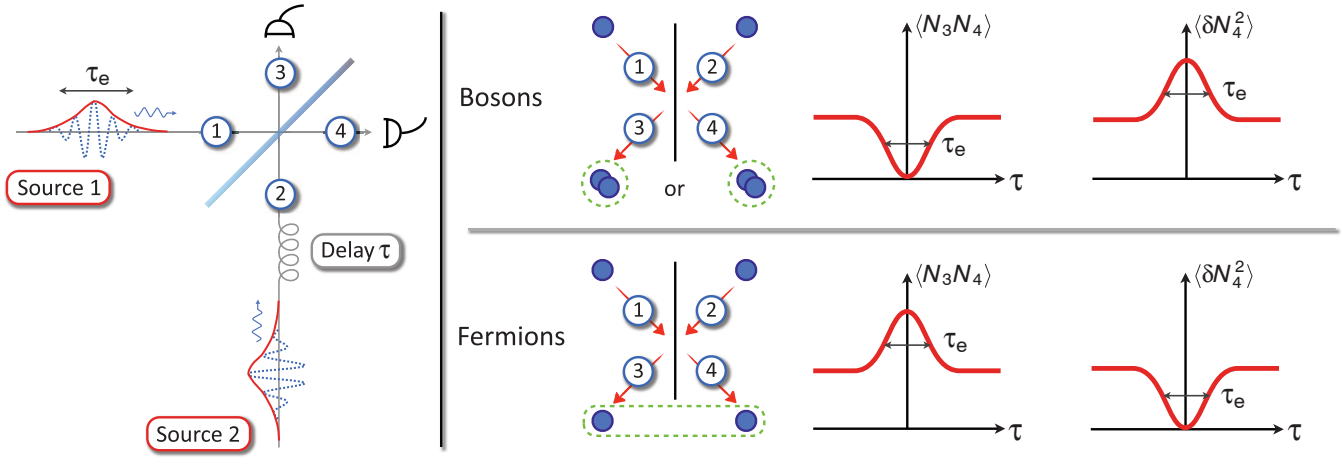

Fig. 1. Sketch of the experiment. Two single-particle wave packets of width τ_e are emitted at inputs 1 and 2 and partitioned on a splitter. Coincident counts $\langle N_3 N_4\rangle$ and fluctuations $\langle\delta N_4^2\rangle$ can be recorded at the outputs 3 and 4 as a function of the tunable delay τ. Indistinguishable bosons always exit in the same output. This results in a suppression of the coincidence count and a doubling of the fluctuations at zero delay compared to the partitioning of classical particles obtained for $\tau >> \tau_e$. An opposite behavior is expected for indistinguishable fermions (doubling of the coincidence counts and suppression of the fluctuations).

time delays. The noise values Δq are normalized by the value of the noise on the plateau. The sum of the partition noises for each source can also be measured by switching off each source alternately. This random partition noise is represented on Fig. 3 by the blurry blue line, whose extension represents the error bar. As expected, it agrees with Δq for large time delays.

The dip observed for short time delay is analogous to the HOM dip but is related here to the antibunching of single indistinguishable fermions; we thus call it the Pauli dip. It reflects our ability to produce single-particle states emitted by two different emitters with some degree of indistinguishability. The states are not perfectly identical, as shown by the fact that the dip does not go to zero. Coulomb repulsion between electrons and between holes on the splitter could also be responsible for a dip in the low-frequency noise. However, this effect can be ruled out by using the long time-delay limit, $\tau \approx 240$ ps. In this limit, the arrival of one electron is synchronized with the arrival of a hole in the other input. A random partitioning is observed (Fig. 3), although Coulomb attraction between electrons and holes would also predict a dip in the low-frequency noise (as the transmitted charge is always zero when electrons and holes exit in the same output). The dip around zero time delay can be well fitted by the expression $\Delta q = 1 - \gamma e^{-\frac{\tau - \tau_0}{\tau_e}}$ expected for two exponentially decaying wave packets but with a non–unit overlap γ. We find $\tau_e = 62 \pm 10$ ps, $\gamma = 0.45 \pm 0.05$, and $\tau_0 = 13 \pm 6$ ps, consistent with the 10-ps accuracy of the synchronization between sources. As noted above, these results can be compared with a numerical simulation of Δq in the Floquet scattering formalism, which we denote $\Delta q_F(\tau)$. For identical emission parameters of both sources, Floquet theory predicts a unit overlap at zero time delay, $\Delta q_F(\tau = 0) = 0$. The red trace in Fig. 3 represents $\Delta q = 1 - \gamma[1 - \Delta q_F(\tau)]$, which imposes a non–unit overlap γ in the Floquet scattering formalism. It reproduces well the shape of the dip with the following parameters: $\gamma = 0.5$, $D_1 = D_2 = 0.4$, $\Delta_1 = \Delta_2 = 1.4$ K, and $T = 100$ mK.

This non–unit overlap can be attributed to two different origins. First, it could stem from some small differences in the emission energies related to small differences in the static potential of each dot. Using Eq. 2, a reduction to a 50% overlap can be obtained by shifting one level relative to the other by energy $\Delta/10$. The value of the static potential is fixed with a better accuracy, but small variations could occur within the several hours of measurement time for each point. The second possibility is related to the decoherence of single-electron wave packets during propagation toward the splitter (which could arise from Coulomb interaction with the adjacent edge channel). In a simple treatment of the wave-packet decoherence, the pure state $\phi_1(t)$ is replaced by the density matrix $\rho_1(t,t') = \phi_1(t)\phi_1^*(t')\mathcal{D}_1(t,t')$, where $\mathcal{D}_1(t,t')$ is a decoherence factor (*27*, *29*). We have $\mathcal{D}_1(t,t) = 1$, such that the average current $\langle I(t) \rangle$ is not affected, but $\mathcal{D}_1(t,t') \to 0$ for $|t - t'| \to \infty$, suppressing the coherence of the electronic wave packet. In that case, Eq. 2 becomes

$$\Delta q = 1 - \mathrm{Tr}[\rho_1\, \rho_2] \quad (4)$$

$$= 1 - \int dt dt' \phi_1(t)\phi_1^*(t')\mathcal{D}_1(t,t') \times \phi_2^*(t)\phi_2(t')\mathcal{D}_2(t,t') \quad (5)$$

Equation 5 exemplifies the fact that the noise suppression stems from a two-particle interference effect encoded in the off-diagonal components of the density matrices ρ_i, i.e., on the coherence of the electronic wave packet. Assuming $\mathcal{D}_1(t,t') = \mathcal{D}_2(t,t') = e^{-\frac{|t-t'|}{\tau_c}}$ in Eq. 5, we find analytically that the overlap depends on the ratio between the intrinsic coherence time of the wave packet τ_e and the coherence time τ_c associated with the propagation along the edge: $\gamma = \frac{\tau_c/(2\tau_e)}{1+\tau_c/(2\tau_e)}$. For $\tau_e \ll \tau_c$, the effects of decoherence can be neglected but in the opposite limit, $\tau_c \ll \tau_e$, the overlap is completely suppressed and the classical partitioning is recovered. In this case, electrons are rendered distinguishable through their interaction with the environment. Within this picture, our measurement of the overlap is compatible with $\tau_c \approx 100$ ps. Such decoherence effects underline the necessity to reach the subnanosecond time scale in electron emission to be able to generate indistinguishable electron wave packets.

The observed Pauli dip in the low-frequency noise of the output current for short time delays

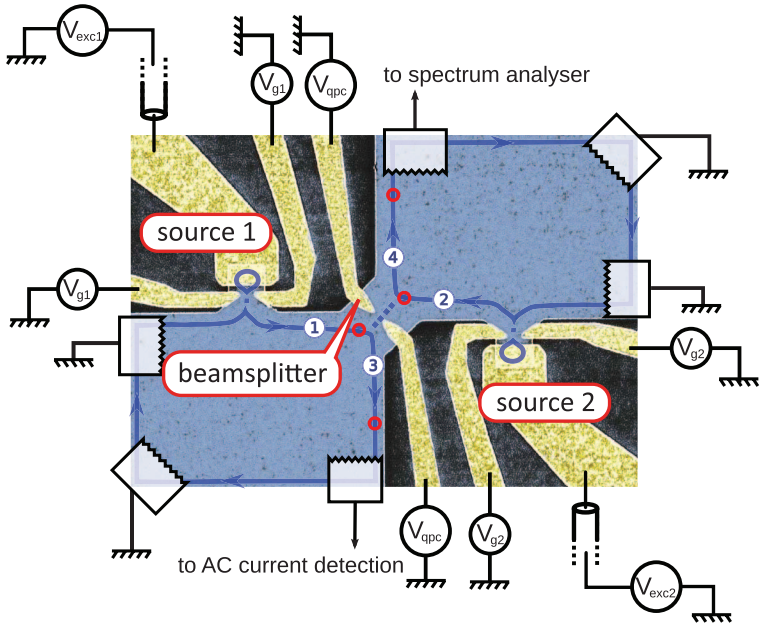

Fig. 2. Sketch of the sample based on a scanning electron microscope image. The electron gas is represented in blue. Two single-electron emitters are located at inputs 1 and 2 of a quantum point contact used as a single-electron beam splitter. Transparencies D_1 and D_2 and static potentials of dots 1 and 2 are tuned by gate voltages $V_{g,1}$ and $V_{g,2}$. Electron and hole emissions are triggered by excitation drives $V_{exc,1}$ and $V_{exc,2}$. The transparency of the beam splitter partitioning the inner edge channel (blue line) is tuned by gate voltage V_{qpc} and set at $\mathcal{T} = 1/2$. The average ac current generated by sources 1 and 2 is measured on output 3, and the low-frequency output noise S_{44} is measured on output 4.

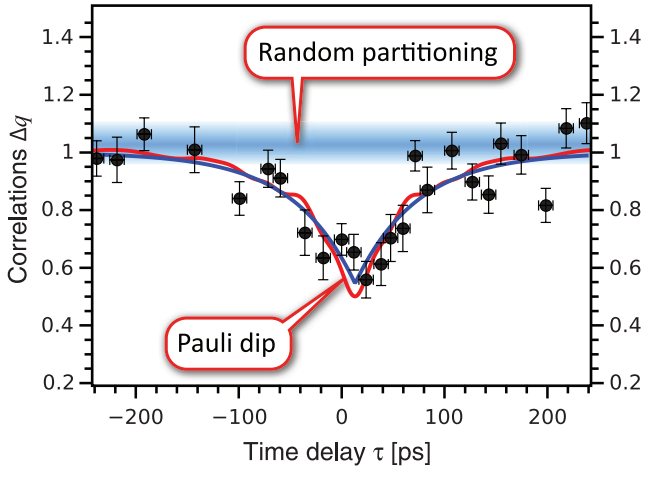

Fig. 3. Excess noise Δq as a function of the delay τ and normalized by the value on the plateau observed for long delays. The blurry blue line represents the sum of the partition noise of both sources. The blue trace is an exponential fit by $\Delta q = 1 - \gamma e^{-\frac{|\tau - \tau_0|}{\tau_e}}$. The red trace is obtained by using Floquet scattering theory, which includes finite temperature effects.

Downloaded from www.sciencemag.org on March 21, 2013

between the arrival times of electrons at a beam splitter is a signature of two-particle interference, which demonstrates the possibility of generating coherent and indistinguishable single-electron wave packets with independent sources. It provides the possibility of controlled manipulation of single-electron states in quantum conductors, with applications in quantum information processing, but could also be used to fully reconstruct the wave function of a single electron (*24*, *30*) and thus quantitatively address the propagation of a single excitation propagating in a complex environment.

References and Notes

1. Y. Ji *et al.*, *Nature* **422**, 415 (2003).
2. P. Roulleau *et al.*, *Phys. Rev. Lett.* **100**, 126802 (2008).
3. M. Yamamoto *et al.*, *Nat. Nanotechnol.* **7**, 247 (2012).
4. Y. Blanter, M. Büttiker, *Phys. Rep.* **336**, 1 (2000).
5. E. Knill, R. Laflamme, G. J. Milburn, *Nature* **409**, 46 (2001).
6. A. Bertoni, P. Bordone, R. Brunetti, C. Jacoboni, S. Reggiani, *Phys. Rev. Lett.* **84**, 5912 (2000).
7. C. K. Hong, Z. Y. Ou, L. Mandel, *Phys. Rev. Lett.* **59**, 2044 (1987).
8. J. Beugnon *et al.*, *Nature* **440**, 779 (2006).
9. R. C. Liu, B. Odom, Y. Yamamoto, S. Tarucha, *Nature* **391**, 263 (1997).
10. P. Samuelsson, E. V. Sukhorukov, M. Büttiker, *Phys. Rev. Lett.* **92**, 02685 (2004).
11. I. Neder *et al.*, *Nature* **448**, 333 (2007).
12. G. Fève *et al.*, *Science* **316**, 1169 (2007).
13. M. D. Blumenthal *et al.*, *Nat. Phys.* **3**, 343 (2007).
14. C. Leicht *et al.*, *Semicond. Sci. Technol.* **26**, 055010 (2011).
15. S. Hermelin *et al.*, *Nature* **477**, 435 (2011).
16. R. P. G. McNeil *et al.*, *Nature* **477**, 439 (2011).
17. A. Mahé *et al.*, *Phys. Rev. B* **82**, 201309(R) (2010).
18. M. Albert, C. Flindt, M. Büttiker, *Phys. Rev. B* **82**, 041407(R) (2010).
19. T. Jonckheere, T. Stoll, J. Rech, T. Martin, *Phys. Rev. B* **85**, 045321 (2012).
20. F. D. Parmentier *et al.*, *Phys. Rev. B* **85**, 165438 (2012).
21. E. Bocquillon *et al.*, *Phys. Rev. Lett.* **108**, 196803 (2012).
22. M. Henny *et al.*, *Science* **284**, 296 (1999).
23. W. D. Oliver, J. Kim, R. C. Liu, Y. Yamamoto, *Science* **284**, 299 (1999).
24. C. Grenier *et al.*, *New J. Phys.* **13**, 093007 (2011).
25. T. Jonckheere, J. Rech, C. Wahl, T. Martin, *Phys. Rev. B* **86**, 125425 (2012).
26. S. Ol'khovskaya, J. Splettstoesser, M. Moskalets, M. Büttiker, *Phys. Rev. Lett.* **101**, 166802 (2008).
27. G. Fève, P. Degiovanni, T. Jolicoeur, *Phys. Rev. B* **77**, 035308 (2008).
28. M. Moskalets, P. Samuelsson, M. Büttiker, *Phys. Rev. Lett.* **100**, 086601 (2008).
29. P. Degiovanni, C. Grenier, G. Fève, *Phys. Rev. B* **80**, 241307(R) (2009).
30. G. Haack, M. Moskalets, J. Splettstoesser, M. Büttiker, *Phys. Rev. B* **84**, 081303 (2011).

Acknowledgments: This work is supported by the Agence Nationale de la Recherche grant "1shot," ANR-2010-BLANC-0412.

9 November 2012; accepted 18 December 2012
Published online 24 January 2013;
10.1126/science.1232572

InP Nanowire Array Solar Cells Achieving 13.8% Efficiency by Exceeding the Ray Optics Limit

Jesper Wallentin,[1] Nicklas Anttu,[1] Damir Asoli,[2] Maria Huffman,[2] Ingvar Åberg,[2] Martin H. Magnusson,[2] Gerald Siefer,[3] Peter Fuss-Kailuweit,[3] Frank Dimroth,[3] Bernd Witzigmann,[4] H. Q. Xu,[1,5] Lars Samuelson,[1] Knut Deppert,[1] Magnus T. Borgström[1]*

Photovoltaics based on nanowire arrays could reduce cost and materials consumption compared with planar devices but have exhibited low efficiency of light absorption and carrier collection. We fabricated a variety of millimeter-sized arrays of p-type/intrinsic/n-type (p-i-n) doped InP nanowires and found that the nanowire diameter and the length of the top n-segment were critical for cell performance. Efficiencies up to 13.8% (comparable to the record planar InP cell) were achieved by using resonant light trapping in 180-nanometer-diameter nanowires that only covered 12% of the surface. The share of sunlight converted into photocurrent (71%) was six times the limit in a simple ray optics description. Furthermore, the highest open-circuit voltage of 0.906 volt exceeds that of its planar counterpart, despite about 30 times higher surface-to-volume ratio of the nanowire cell.

Nanostructures are currently being investigated for next-generation photovoltaic (PV) architectures as a means of lowering cost (*1*) through the use of abundant materials (*2*) or to improve light trapping (*3*). Nanowire (NW) arrays could provide substantial reductions in material consumption as well as production costs for III-V-based solar cells, in part because they can be monolithically grown on low-cost substrates such as silicon (*4*). However, proof of concepts of III-V NW-based PV (*5*–*9*), have had limited efficiencies in the 3 to 5% range.

The efficiency of NW-based solar cells is often limited by light absorption, especially when the NWs have subwavelength dimensions. In a ray optics description, the maximum fraction of normally incident sunlight that could be absorbed and converted to a photocurrent is proportional to the surface coverage of the active material. However, theoretical modeling based on wave optics has predicted resonant light trapping in sub-200-nm-diameter NW arrays (*10*–*12*), which would allow bulklike photocurrent generation with just a fraction of the materials consumption. Experimental studies have been confined to NW arrays with either large-diameter wires (*13*, *14*) or high surface coverage (*9*). Another limitation is that crystal surfaces typically have a high density of defects that act as potential recombination centers, and nanostructured devices have high surface-to-volume (S/V) ratios. Surface recombination could explain the hitherto observed relatively low open-circuit voltages (V_{oc}) in NW-based PV cells (*8*, *9*).

Here, we demonstrate how these challenges can be overcome and report on a NW array solar cell with 13.8% efficiency. Although the 180-nm-diameter InP NWs only cover 12% of the surface, they deliver 83% of the photocurrent density obtained in planar InP solar cells (*15*, *16*). Furthermore, the highest V_{oc} exceeds that of the InP planar record cell (*15*, *16*), despite about 30 times higher S/V ratio in our NW-based PV cell. By using three-dimensional (3D) optical modeling, we provide insight into the origins of the high performance of our solar cells, as well as guidelines to how they further can be improved.

We chose InP not only because of its direct band gap of 1.34 eV (925 nm wavelength-equivalent), suitable for the solar spectrum but also because it allows in situ etching with HCl during NW growth to prevent short-circuiting from radial overgrowth (*17*). The InP NWs in our solar cells were epitaxially grown with an axially defined p-type/intrinsic/n-type (p-i-n) doped structure (*7*) and have a length of ~1.5 μm. We used a nanoimprint technique to arrange gold seed particles in arrays (*18*). (Fig. 1, A to C). Different sizes and array pitches of the Au seeds were used, resulting in samples with different NW diameters (130 to 190 nm) and array pitches (470 or 500 nm). To reduce reflection, we removed the metal seed particles after growth by using wet etching and defined a top contact with a silicon oxide insulating layer and a transparent conducting oxide (TCO) (*7*). Last, the 1-mm-by-1-mm cells and metal contact pads were defined with optical lithography (Fig. 1C), with each sample containing a few solar cells. Details of the samples (table S1) and their fabrication are given in the supplementary materials (*19*).

Characterization of the solar cells (Fig. 1D) revealed very good performance in comparison with other InP PV architectures (Table 1). At 1-sun

[1]Solid State Physics, Lund University, Box 118, 22100 Lund, Sweden. [2]Sol Voltaics AB, Ideon Science Park, Scheelevägen 17, 22370 Lund, Sweden. [3]Fraunhofer ISE, Heidenhofstrasse 2, D-79110 Freiburg, Germany. [4]University of Kassel, Wilhelmshoeher Allee 71, 34121, Kassel, Germany. [5]Key Laboratory for the Physics and Chemistry of Nanodevices and Department of Electronics, Peking University, Beijing 100871, China.

*To whom correspondence should be addressed. E-mail: magnus.borgstrom@ftf.lth.se

Downloaded from www.sciencemag.org on March 21, 2013